



1 **GPU-HADVPPM4HIP V1.0: higher model accuracy on China's**  
2 **domestically GPU-like accelerator using heterogeneous compute**  
3 **interface for portability (HIP) technology to accelerate the piecewise**  
4 **parabolic method (PPM) in an air quality model (CAMx V6.10)**

5 **Kai Cao<sup>1</sup>, Qizhong Wu<sup>1,5</sup>, Lingling Wang<sup>2</sup>, Hengliang Guo<sup>3</sup>, Nan Wang<sup>2</sup>, Huaqiong Cheng<sup>1,5</sup>,**  
6 **Xiao Tang<sup>4</sup>, Lina Liu<sup>3</sup>, Dongqing Li<sup>1</sup>, Hao Wu<sup>3</sup>, and Lanning Wang<sup>1,5</sup>**

7 <sup>1</sup>College of Global Change and Earth System Science, Faculty of Geographical Science, Beijing  
8 Normal University, Beijing 100875, China

9 <sup>2</sup>Henan Ecological Environmental Monitoring Centre and Safety Center, Henan Key Laboratory  
10 of Environmental Monitoring Technology, Zhengzhou 450008, China

11 <sup>3</sup>National Supercomputing Center in Zhengzhou, Zhengzhou, 450001, China

12 <sup>4</sup>State Key Laboratory of Atmospheric Boundary Layer Physics and Atmospheric Chemistry,  
13 Institute of Atmospheric Physics, Chinese Academy of Science, Beijing 100029, China

14 <sup>5</sup>Joint Center for Earth System Modeling and High Performance Computing, Beijing Normal  
15 University, Beijing, 100875, China

16

17 **Correspondence to:** Qizhong Wu ([wqizhong@bnu.edu.cn](mailto:wqizhong@bnu.edu.cn)); Lingling

18 Wang([928216422@qq.com](mailto:928216422@qq.com)); Lanning Wang ([wangln@bnu.edu.cn](mailto:wangln@bnu.edu.cn))

19

20 **Abstract.** The graphics processing units (GPUs) are becoming a compelling acceleration strategy  
21 for geoscience numerical model due to their powerful computing performance. In this study, AMD's  
22 heterogeneous compute interface for portability (HIP) was implemented to port the GPU  
23 acceleration version of the Piecewise Parabolic Method (PPM) solver (GPU-HADVPPM) from the  
24 NVIDIA GPUs to China's domestically GPU-like accelerators as GPU-HADVPPM4HIP, and  
25 further introduced the multi-level hybrid parallelism scheme to improve the total computational  
26 performance of the HIP version of CAMx (CAMx-HIP) model on the China's domestically  
27 heterogeneous cluster. The experimental results show that the acceleration effect of GPU-  
28 HADVPPM on the different GPU accelerator is more obvious when the computing scale is larger,



29 and the maximum speedup of GPU-HADVPPM on the domestic GPU-like accelerator is 28.9 times.  
30 The hybrid parallelism with a message passing interface (MPI) and HIP enables achieve up to 17.2  
31 times speedup when configure 32 CPU cores and GPU-like accelerators on the domestic  
32 heterogeneous cluster. And the OpenMP technology is introduced to further reduce the computation  
33 time of CAMx-HIP model by 1.9 times. More importantly, by comparing the simulation results of  
34 GPU-HADVPPM on NVIDIA GPUs and domestic GPU-like accelerators, it is found that the  
35 simulation results of GPU-HADVPPM on domestic GPU-like accelerators have less difference than  
36 the NVIDIA GPUs, and the reason for this difference may be related to the fact that the NVIDIA  
37 GPU sacrifices part of the accuracy for improved computing performance. All in all, the domestic  
38 GPU-like accelerators are more accuracy for scientific computing in the field of geoscience  
39 numerical models. Furthermore, we also exhibit that the data transfer efficiency between CPU and  
40 GPU has an important impact on heterogeneous computing, and point out that optimizing the data  
41 transfer efficiency between CPU and GPU is one of the important directions to improve the  
42 computing efficiency of geoscience numerical models in heterogeneous clusters in the future.

## 43 1. Introduction

44 Over the recent years, GPUs have become an essential part of providing processing power for  
45 high performance computing (HPC) application, and heterogeneous supercomputing based on CPU  
46 processors and GPU accelerators has become the trend of global advanced supercomputing  
47 development. The 61st edition of the top 10 list, released in June 2023, reveals that 80% of advanced  
48 supercomputers adopt the heterogeneous architectures  
49 (<https://www.top500.org/lists/top500/2023/06/>, last access: 20 October 2023), and the Frontier  
50 system equipped with AMD Instinct MI250X GPU at the Oak Ridge National Laboratory remains  
51 the only true exascale machine with the High-Performance Linpack benchmark (HPL) score of  
52 1.194 Exaflop/s ([https://www.top500.org/news/frontier-remains-sole-exaflop-machine-and-retains-  
53 top-spot-improving-upon-its-previous-hpl-score/](https://www.top500.org/news/frontier-remains-sole-exaflop-machine-and-retains-top-spot-improving-upon-its-previous-hpl-score/), last access: 20 October 2023). It is worth noting  
54 that in addition to the second-place Fugaku supercomputer using a general-purpose CPU  
55 architecture, the third-ranked LUMI system also uses AMD Instinct MI250X GPUs as accelerators  
56 and its HPL score reaches 309.1 PFlop/s. The much-watched AMD Instinct MI250X GPU achieves



57 95.7 TFlop/s for peak double precision matrix performance  
58 (<https://www.amd.com/en/products/server-accelerators/Instinct-mi250x>, last access: 20 October  
59 2023), and its performance is 2.7 times that of EARTH-SIMULATOR which is the top 1  
60 supercomputer in 2003. How to realize the large-scale parallel computing and improve the  
61 computational performance of geoscience numerical models on the GPU has become one of the  
62 significant directions for the future development of numerical models.

63 In terms of the heterogeneous porting for the atmospheric chemical models, many scholars  
64 have carried out research on chemical modules. For example, Sun et al. (2018) used CUDA  
65 technology to port the second-order Rosenbrock solver of chemistry module of CAM4-Chem to  
66 NVIDIA Tesla K20X GPU and achieved up 11.7x speedup for computation alone. Alvanos and  
67 Christoudias (2017) developed a software that automatically generates CUDA kernels to solve  
68 chemical kinetics equation in the chemistry module for the global climate model ECHAM/MESy  
69 Atmospheric Chemistry (EMAC) and performance evaluation shows a 20.4x speedup for the kernel  
70 execution. Linford et al. (2011) presented the Kinesthetic PreProcessor: Accelerated (KPPA) to  
71 generate the chemical mechanism code in CUDA language which can be implemented on NVIDIA  
72 Tesla C1060 GPU. The KPPA-generated SAPRC'99 mechanism from CMAQ model achieved a  
73 maximum speedup of 13.7x and KPPA-generated RADM2 mechanism from WRF-chem model  
74 achieved an 8.5x speedup over the serial implementation. Horizontal advection module for the  
75 atmospheric chemical models, Cao et al. (2023) used the Fortran-C-CUDA C scheme and  
76 implemented a series of optimizations, including reduce the CPU–GPU communication frequency,  
77 optimize the GPU memory access, and thread and block co-indexing, to increase the computational  
78 efficiency of the HADVPPM advection solver in the CAMx model by 18.8 times on the NVIDIA  
79 Tesla V100 GPU.

80 The CUDA technology was implemented to carry out heterogeneous porting for the  
81 atmospheric chemical models from the CPU processors to different NVIDIA GPU accelerators. In  
82 this study, the Heterogeneous-computing Interface for Portability (HIP) interface was introduced to  
83 implement the porting of GPU-HADVPPM from the NVIDIA GPU to the China's domestically  
84 GPU-like accelerators based on the research of Cao et al. (2023). First, we compared the simulation  
85 result of Fortran version CAMx model with CUDA version of CAMx (CAMx-CUDA) and CAMx-



86 HIP model which were coupled with CUDA and HIP version of GPU-HADVPPM program,  
87 respectively. And then, the computing performance of GPU-HADVPPM programs on different  
88 GPUs are compared. Finally, we tested total coupling performance of CAMx-HIP model with multi-  
89 level hybrid parallelization on the China's domestically heterogeneous cluster.

## 90 **2. Model and experimental platform**

### 91 **2.1. The CAMx model description and configuration**

92 The Comprehensive Air Quality Model with Extensions version 6.10 (CAMx v6.10;  
93 ENVIRON, 2014) is a state-of-the-art air quality model which simulates the emission, dispersion,  
94 chemical reaction, and removal of the air pollutants on a system of nested three-dimensional grid  
95 boxes (<https://www.camx.com/>, last access: last access: 20 October 2023). The Eulerian continuity  
96 equation is expressed as shown Cao et al. (2023), the first term on the right-hand side represents  
97 horizontal advection, the second term represents net resolved vertical transport across an arbitrary  
98 space and time varying height grid, and the third term represents turbulent diffusion on the sub-grid  
99 scale. Pollutant emission represents both point source emissions and grided source emissions.  
100 Chemistry is treated by solving a set of reaction equations defined by specific chemical mechanisms.  
101 Pollutant removal includes both dry deposition and wet scavenging by precipitation.

102 In terms of the horizontal advection term on the right-hand side, this equation is solved using  
103 either the Bott (1989) scheme or the Piecewise Parabolic Method (PPM) (Colella and Woodward,  
104 1984; Odman and Ingram, 1996) scheme. The PPM horizontal advection scheme (HADVPPM) was  
105 selected in this study because it provides higher accuracy with minimal numerical diffusion. The  
106 other numerical scheme selected during the CAMx model running are listed in Table S1. As  
107 described by Cao et al. (2023), the -fp-model precise compile flag which can force the compiler to  
108 use the vectorization of some computation under value safety is 41.4% faster than -mieee-fp compile  
109 flag which comes from the Makefile of the official CAMx version with the absolute errors of the  
110 simulation results are less than  $\pm 0.05$  ppbV. Therefore, the -fp-model precise compile flag was  
111 selected when compiling the CAMx model in this research.



## 112 2.2. CUDA and ROCm introduction

113 Compute Unified Device Architecture (CUDA) (NVIDIA, 2020) is a parallel programming  
114 paradigm which was released in 2007 by NVIDIA. CUDA is a proprietary application programming  
115 interface (API) and as such is only supported on NVIDIA's GPUs that are based on Tesla  
116 Architecture. For the CUDA programming, it uses a programming language similar to standard C,  
117 which achieves efficient parallel computing of programs on NVIDIA GPUs by adding some  
118 keywords. In the previous study, CUDA technology was implemented to port the HADVPPM  
119 program from CPU to NVIDIA GPU (Cao et al., 2023).

120 Radeon Open Compute platform (ROCm) (AMD, 2023) is an open-source software platform  
121 developed by AMD in 2015 for HPC and hyperscale GPU computing. In general, ROCm for the  
122 AMD GPU is equivalent to CUDA for NVIDIA GPU. On the ROCm software platform, it uses the  
123 AMD's HIP interface which is a C++ runtime API to allows developers to run programs on AMD  
124 GPUs. Table 1 shows the difference between the CUDA programming and HIP programming on the  
125 NVIDIA GPU and AMD GPU. In general, it is very similar between the CUDA and HIP  
126 programming and their code can be converted directly by replacing the character "cuda" with "hip"  
127 in the most cases. More information about HIP API can be available on  
128 <https://rocm.docs.amd.com/projects/HIP/en/latest/index.html> (last access: 20 October 2023).  
129 Similar to AMD GPU, developers can also use ROCM-HIP programming interface to implement  
130 programs running on the China's domestically GPU-like accelerator.

131 **Table 1.** The difference between the CUDA programming and HIP programming on the NVIDIA GPU and AMD  
132 GPU.

	CUDA programming	HIP programming
Header file	cuda_runtime.h	hip_runtime.h
Gets the number of compute-capable GPUs.	cudaGetDeviceCount	hipGetDeviceCount
Set device to be used for GPU executions.	cudaSetDevice	hipSetDevice
Allocates memory on the GPU.	cudaMalloc	hipMalloc
Copies data between CPU and GPU.	cudaMemcpy	hipMemcpy



---

Kernel function	mykernel<<< >>>	hipLaunchKernelGGL(mykernel)
Frees memory on the GPU.	cudaFree	hipFree

---

133

### 134 **2.3. Hardware components and software environment of the testing system**

135 Table 2 listed four GPU clusters which are conducted the experiments, two NVIDIA  
136 heterogeneous clusters which have the same hardware configuration as Cao et al. (2023) and two  
137 China's domestically heterogeneous clusters newly used in this research. The NVIDIA K40m  
138 cluster is equipped with two 2.5 GHz 16 cores Intel Xeon E5-2682 v4 CPU and one NVIDIA Tesla  
139 K40m GPU. Each NVIDIA Tesla K40m GPU accelerator has 2880 CUDA cores with 12 GB of  
140 video memory. The NVIDIA V100 cluster contains two 2.7 GHz 24 cores Intel Xeon Platinum 8168  
141 processors and eight NVIDIA Tesla V100 GPU accelerators. Each NVIDIA Tesla V100 GPU  
142 accelerator is configured with 5120 CUDA cores and 16 GB video memory.

143 For the China's domestically heterogeneous cluster A (domestic cluster A), each compute node  
144 contains a 2.0 GHz China's domestically CPU processor A of 32 cores (domestic CPU processor  
145 A) and four China's domestically GPU-like accelerator A (domestic GPU-like accelerator A). Each  
146 CPU processor A has 32 cores with 4 Non-Uniform Memory Access nodes, each NUMA node has  
147 8 X86 based processors. The GPU-like accelerator A has 64 compute unit, for totaling 60 threads  
148 on each compute unit. The China's domestically heterogeneous cluster B (domestic cluster B) is  
149 the next generation of cluster A, and its CPU and GPU hardware have been upgraded, especially the  
150 data transfer bandwidth between CPU and GPU. The CPU and GPU configuration scheme on the  
151 cluster B is the same as the cluster B, with one 2.5 GHz China's domestically CPU processor B  
152 (domestic CPU processor B) on a single node equipped with four China's domestically GPU-like  
153 accelerator B (domestic GPU-like accelerator B). The domestic GPU-like accelerator B also  
154 contains 64 compute units with 128 threads each.

155 In term of the software environment, the Intel Toolkit (including compiler and MPI library)  
156 version 2021.4.0, 2019.1.144, and 2021.3.0 are employed for compiling on Intel CPU and China's  
157 domestically series CPU, respectively. The drivers and libraries of NVIDIA Tesla K40m and V100  
158 GPU accelerator, domestic GPU-like accelerator A and B were CUDA version 10.2, CUDA version



159 10.0, ROCm version 4.0.1/ DTK toolkit version 23.04, and DTK toolkit version 23.04. DTK toolkit,  
 160 like ROCm, supports developers to develop GPU-like applications using HIP programming  
 161 interface in C++ language.

162 **Table 2.** Configurations of NVIDIA K40m cluster, NVIDIA V100 cluster, China’s domestically cluster A, and China’s  
 163 s domestically cluster B.

	Hardware components	
	CPU	GPU
NVIDIA K40m cluster	Intel Xeon E5-2682 v4 CPU @2.5 GHz, 16 cores	NVIDIA Tesla K40m GPU, 2880 CUDA cores, 12 GB video memory
NVIDIA V100 cluster	Intel Xeon Platinum 8168 CPU @2.7 GHz, 24 cores	NVIDIA Tesla V100 GPU, 5120 CUDA cores, 16 GB video memory
China’s domestically cluster A	China’s domestically CPU processor A, 2.0GHz, 32 cores	China’s domestically GPU-like accelerator A, 3840 stream processors, 16 GB memory
China’s domestically cluster B	China’s domestically CPU processor B, 2.5GHz, 32 cores	China’s domestically GPU-like accelerator B, 8192 stream processors, 16 GB memory
	Software environment	
	Compiler and MPI	Programming model
NVIDIA K40m cluster	Intel Toolkit 2021.4.0	CUDA-10.2
NVIDIA V100 cluster	Intel Toolkit 2019.1.144	CUDA-10.0
China’s domestically cluster A	Intel Toolkit 2021.3.0	ROCm-4.0.1/ DTK-23.04
China’s domestically cluster B	Intel Toolkit 2021.3.0	DTK-23.04

164

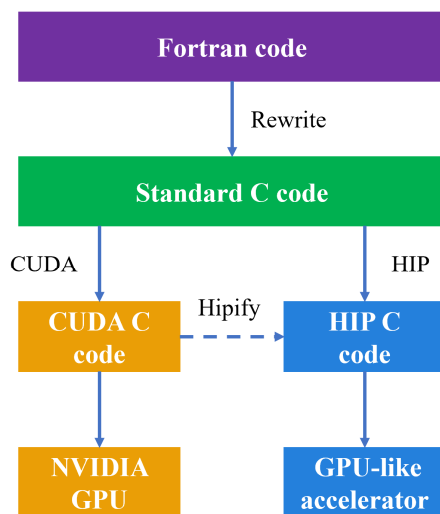
### 165 3. Implementation details

166 This section mainly introduced the strategy of porting HADVPPM program from CPU to  
 167 NVIDIA GPU and domestic GPU-like accelerator, as well as the proposed multi-level hybrid  
 168 parallelism technology to make full use of computing resources.



169 **3.1. Porting the HADVPPM program from CPU to NVIDIA GPU and domestic**  
170 **GPU-like accelerator**

171 Fig. 1 shows the heterogeneous porting process of HADVPPM from CPU to NVIDIA GPU  
172 and domestic GPU-like accelerator. First, the original Fortran code was refactored using standard C  
173 language. And then the CUDA and HIP technology were used to convert the standard C code into  
174 CUDA C and HIP C code to make it computable on the NVIDIA GPU and domestic GPU-like  
175 accelerator. To facilitate the portability of applications across different GPU platforms, ROCm  
176 provides hipify toolkits to help transcode. In this studying, the ROCm HIP technology was used to  
177 implement the operation of GPU-HADVPPM on domestic GPU-like accelerator based on the  
178 CUDA version of GPU-HADVPPM which was developed by Cao et al. (2023). During the  
179 compiling, the HIP code was compiled using the “hipcc” compiler driver with the library flag “-  
180 lamdhip64”.



181  
182 **Figure 1.** The heterogeneous porting process of HADVPPM Fortran code from CPU to NVIDIA GPU and domestic  
183 GPU-like accelerator.  
184





### 185 **3.2. Multi-level hybrid parallelization of CAMx model on heterogeneous** 186 **platform**

187 The original CAMx model running on the CPUs supports two types of parallelization  
188 (ENVIRON, 2014): (1) OpenMP (OMP), which supports multi-platform (e.g., multi-core) shared-  
189 memory programming in C/C++ and Fortran; (2) Message Passing Interface (MPI), which is a  
190 message passing interface standard for developing and running parallel applications on the  
191 distributed-memory computer cluster. In the original CAMx model, MPI+OMP hybrid parallel can  
192 be used to maximize computational efficiency.

193 In the previous studying, Cao et al. (2023) adopt a parallel architecture with an MPI and CUDA  
194 (MPI+CUDA) hybrid paradigm to expand the parallel scale of CAMx-CUDA model in NVIDIA  
195 heterogeneous cluster. Adopting this strategy, GPU-HADVPPM can run on multiple NVIDIA GPUs.  
196 When the CUDA C code of GPU-HADVPPM is converted to HIP C code, GPU-HADVPPM with  
197 an MPI and HIP (MPI+HIP) heterogeneous hybrid programming technology can also run on  
198 multiple domestic GPU-like accelerators. The MPI and HIP hybrid parallel scheme can configure  
199 one GPU-like accelerator for each CPU process participating in the computation. However, the  
200 number of GPU-like accelerators in a single compute node is usually much smaller than the number  
201 of CPU cores in the super-large heterogeneous cluster. Therefore, in order to make full use of the  
202 remaining CPU computing resources, OMP technology is further introduced into the CAMx-HIP  
203 model which was coupled the HIP version of GPU-HADVPPM. In the framework of the multi-level  
204 hybrid parallelism, the horizontal advection module is accelerated by MPI and HIP technology, and  
205 the other modules are accelerated by MPI and OMP.

## 206 **4. Results and evaluation**

207 The coupling performance experiments of CUDA and HIP version GPU-HADVPPM were  
208 conducted in this section. First, we compared the simulation result of Fortran version CAMx model  
209 with CAMx-CUDA and CAMx-HIP model which were coupled with CUDA and HIP version of  
210 GPU-HADVPPM program, respectively. Then, the computing performance of GPU-HADVPPM  
211 programs on the NVIDIA GPU and domestic GPU-like accelerator are compared. Finally, we tested



212 total coupling performance of CAMx-HIP model with multi-level hybrid parallelization on the  
213 domestic cluster A. For ease of description, the CAMx versions of the HADVPPM program written  
214 in Fortran, CUDA C and HIP C code are named F, CUDA and HIP, respectively.

#### 215 4.1. Experimental setup

216 There are three test cases were used to evaluate the coupling performance of CUDA and HIP  
217 version GPU-HADVPPM. The experimental setup for the three test cases is shown in Table 3. The  
218 Beijing case (BJ) covers Beijing, Tianjin, and part of the Hebei Province with  $145 \times 157$  grid  
219 boxes, and simulation of BJ case starts on 1 November, 2020. The Henan case (HN) mainly covers  
220 the Henan Province with  $209 \times 209$  grid boxes. The starting date of simulation in HN case is 1  
221 October, 2022. The Zhongyuan case (ZY) has the widest coverage of the three cases, with Henan  
222 Province as the center, covering the Beijing-Tianjin-Hebei region, Shanxi Province, Shaanxi  
223 Province, Hubei Province, Anhui Province, Jiangsu Province, and Shandong Province, with  $531 \times$   
224  $513$  grid boxes. ZY case started simulation on 4 January, 2023. All of the three performance test  
225 cases are 3km horizontal resolution, 48 hours of simulation, and 14 vertical model layers. The  
226 number of three-dimensional grid boxes in BJ, HN, and ZY cases are totally 318,710, 611,534 and  
227 3,813,642, respectively. The meteorological fields inputting the different versions of the CAMx  
228 model in the three cases were provided by the Weather Research and Forecasting Model (WRF). In  
229 terms of emission inventories, the emission for BJ case is consistent with the Cao et al. (2023), HN  
230 case uses the Multi-resolution Emission Inventory for China (MEIC) and ZY case uses the emission  
231 constructed by Sparse Matrix Operator Kernel Emission (SMOKE) model in this study.

232 **Table 3.** The experimental setup for the BJ, HN, and ZY case.

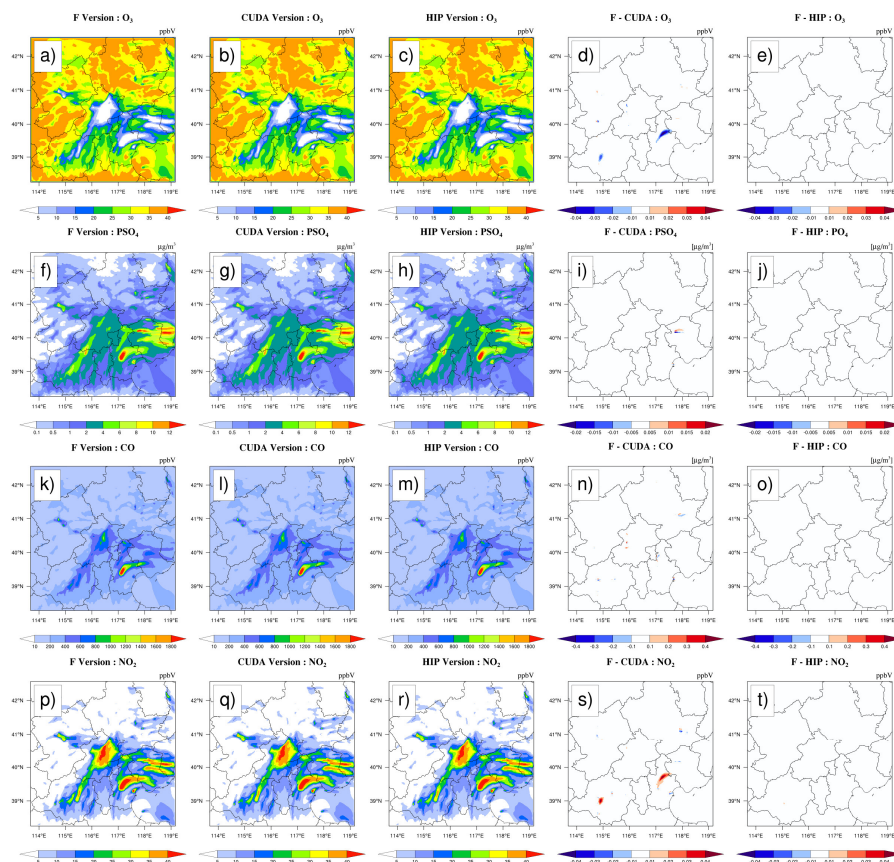
	BJ	HN	ZY
<b>Start date</b>	November 1, 2020	October 1, 2022	1 January, 2023
<b>Horizontal resolution</b>	3km	3km	3km
<b>Grid boxes</b>	$145 \times 157 \times 14$	$209 \times 209 \times 14$	$531 \times 513 \times 14$
<b>Meteorological fields</b>	WRF	WRF	WRF
<b>Emission</b>	Cao et al. (2023)	MEIC	SMOKE

233



## 234 4.2. Error analysis

235 The hourly concentrations of four major species, i.e. O<sub>3</sub>, PSO<sub>4</sub>, CO, and NO<sub>2</sub>, outputted by  
236 Fortran, CUDA, and HIP version of CAMx for the BJ case are compared to verify the results  
237 reasonableness before testing the computation performance. Fig. 2 present the four major species  
238 simulation results of three CAMx version, including Fortran version on the Intel E5-2682 v4 CPU,  
239 CUDA version on the NVIDIA K40m cluster and HIP version on the domestic cluster A, after 48  
240 hours integration, as well as the absolute errors (AEs) of their concentrations. The species' spatial  
241 pattern of three CAMx versions on different platform are visually very consistent, and the AEs  
242 between the HIP and Fortran version is much smaller than the CUDA and Fortran version. For  
243 example, the AEs between the CUDA and Fortran version for O<sub>3</sub>, PSO<sub>4</sub>, and NO<sub>2</sub> are in the range  
244 of  $\pm 0.04$  ppbV,  $\pm 0.02 \mu\text{g} \cdot \text{m}^{-3}$ , and  $\pm 0.04$  ppbV. And the AEs between the HIP and Fortran  
245 version for above the three species are fall into the range of  $\pm 0.01$  ppbV,  $\pm 0.005 \mu\text{g} \cdot \text{m}^{-3}$ , and  
246  $\pm 0.01$  ppbV. For CO, AEs is relatively large due to its high background concentration. However,  
247 the AEs between the HIP and Fortran versions is also less than that between the CUDA and Fortran  
248 versions where were in the range of  $\pm 0.4$  ppbV and  $\pm 0.1$  ppbV, respectively.

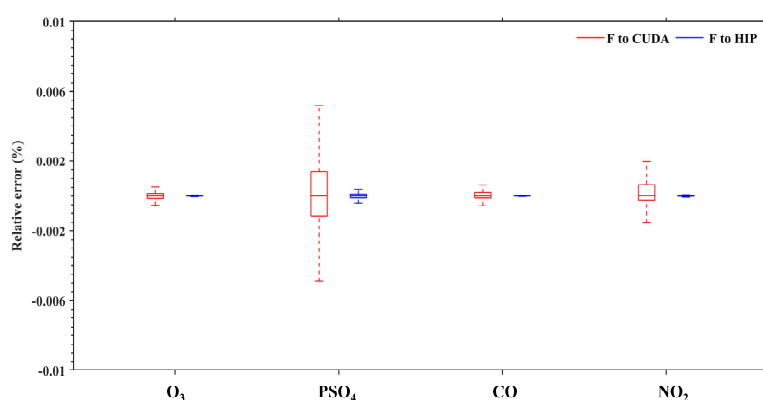


249  
 250 **Figure 2.** O<sub>3</sub>, PSO<sub>4</sub>, CO, and NO<sub>2</sub> concentrations outputted by the CAMx Fortran version on the Intel E5-2682 v4  
 251 CPU, CUDA version on the NVIDIA K40m cluster and HIP version on the domestic cluster A under the BJ case.  
 252 Panels (a), (f), (k), and (p) are from the Fortran version of simulation results for four species. Panels (b), (g), (l), and  
 253 (q) are from the CUDA version of simulation results for four species. Panels (c), (h), (m), and (r) are from the HIP  
 254 version of simulation results for four species. Panels (d), (i), (n), and (s) are the AEs between the Fortran and CUDA  
 255 versions. Panels (e), (j), (o), and (t) are the AEs between the Fortran and HIP versions.

256  
 257 **Fig. 3** presents the boxplot of the relative errors (REs) in all grid boxes for the O<sub>3</sub>, PSO<sub>4</sub>, CO,  
 258 and NO<sub>2</sub> during the 48 hours simulation under the BJ case. Statistically, the REs between the CUDA  
 259 version on the NVIDIA K40m cluster and Fortran version on the Intel E5-2682 v4 CPU for the  
 260 above four species are in the range of  $\pm 0.002\%$ ,  $\pm 0.006\%$ ,  $\pm 0.002\%$ , and  $\pm 0.002\%$ . In terms of



261 REs between the HIP version on the domestic cluster A and Fortran version on the Intel E5-2682 v4  
262 CPU, the values are much smaller than REs between CUDA and Fortran versions which are fall into  
263 the range of  $\pm 0.00006\%$ ,  $\pm 0.0005\%$ ,  $\pm 0.00004\%$ , and  $\pm 0.00008\%$ , respectively.



264  
265 **Figure 3.** The distribution of REs in all grid boxes for the O<sub>3</sub>, PSO<sub>4</sub>, CO, and NO<sub>2</sub> under the BJ case. The red boxplot  
266 represents the REs between the CUDA version on the NVIDIA K40m cluster and Fortran version on the Intel E5-  
267 2682 v4 CPU, and blue boxplot represents the REs between the domestic cluster A and Fortran version on the Intel  
268 E5-2682 v4 CPU.

269  
270 Wang et al. (2021) verified the applicability of the numerical model in scientific research by  
271 computing the ratio of root mean square error (RMSE) between two different model versions to  
272 system spatial variation (standard deviation, std). If the ratio is smaller, it is indicated that the  
273 difference in the simulation results of the model on the GPU is minimal compared with the spatial  
274 variation of the system, that is to say, the simulation results of the model on the GPU are accepted  
275 for scientific research. Here, we compute the standard deviation of O<sub>3</sub>, PSO<sub>4</sub>, CO and NO<sub>2</sub> on the  
276 Intel Xeon E5-2682 v4 CPU, and their root mean square error (RMSE) between the NVIDIA V100  
277 cluster, NVIDIA K40m cluster and domestic cluster A and the Intel Xeon E5-2682 v4 CPU, which  
278 are presented in Table 4. The std for the above four species on the Intel Xeon E5-2682 v4 CPU are  
279 9.6 ppbV, 1.7  $\mu\text{g} \cdot \text{m}^{-3}$ , 141.9 ppbV, and 7.4 ppbV, respectively, and their ratios of RMSE and std  
280 on domestic cluster A are  $5.8 \times 10^{-5}\%$ ,  $4.8 \times 10^{-6}\%$ ,  $5.7 \times 10^{-8}\%$ , and  $2.1 \times 10^{-4}\%$ , which



281 are smaller than two NVIDIA clusters, especially much smaller than the NVIDIA V100 cluster. For  
 282 example, the ratio on the NVIDIA K40m cluster for four species are  $1.2 \times 10^{-4}\%$ ,  $6.6 \times 10^{-5}\%$ ,  
 283  $7.0 \times 10^{-5}\%$ , and  $4.1 \times 10^{-4}\%$ , and ratio on the NVIDIA V100 cluster are  $1.5 \times 10^{-2}\%$ ,  
 284  $2.5 \times 10^{-3}\%$ ,  $6.4 \times 10^{-3}\%$ , and  $1.3 \times 10^{-3}\%$ , respectively.

285 From AEs, REs, and ratio of RMSE and std between different CAMx versions, it can be  
 286 identified that the HIP version of the GPU-HADVPPM program runs on domestic cluster A with  
 287 less difference, and the reason for this difference may be related to the fact that the NVIDIA GPU  
 288 sacrifices part of the accuracy for improved computing performance. In other words, domestic  
 289 cluster A are more accuracy for scientific computing in the field of the geoscience numerical models.  
 290 **Table 4.** The standard deviation (std) of O<sub>3</sub>, PSO<sub>4</sub>, CO and NO<sub>2</sub> on the Intel Xeon E5-2682 v4 CPU, root mean  
 291 square error (RMSE) and its ratio on the NVIDIA V100 cluster, NVIDIA K40m cluster and domestic cluster A

	std	NIVIDA V100 cluster		NIVIDA K40m cluster		domestic cluster A	
		RMSE	RMSE/std	RMSE	RMSE/std	RMSE	RMSE/std
O <sub>3</sub> (ppbV)	9.6	$1.5 \times 10^{-3}$	$1.5 \times 10^{-2}$	$1.1 \times 10^{-5}$	$1.2 \times 10^{-4}$	$7.4 \times 10^{-6}$	$7.7 \times 10^{-5}$
PSO <sub>4</sub> ( $\mu\text{g} \cdot \text{m}^{-3}$ )	1.7	$4.3 \times 10^{-5}$	$2.5 \times 10^{-3}$	$1.1 \times 10^{-6}$	$6.6 \times 10^{-5}$	$2.5 \times 10^{-7}$	$1.5 \times 10^{-5}$
CO (ppbV)	141.9	$9.0 \times 10^{-3}$	$6.4 \times 10^{-3}$	$1.0 \times 10^{-4}$	$7.0 \times 10^{-5}$	$4.4 \times 10^{-7}$	$3.1 \times 10^{-7}$
NO <sub>2</sub> (ppbV)	7.4	$9.3 \times 10^{-5}$	$1.3 \times 10^{-3}$	$3.0 \times 10^{-5}$	$4.1 \times 10^{-4}$	$2.0 \times 10^{-5}$	$2.7 \times 10^{-4}$

292

### 293 4.3. Application performance

#### 294 4.3.1. GPU-HADVPPM on a single GPU accelerator

295 As described in Sect. 4.2, we validate the 48 hours simulation results outputted by the CAMx  
 296 model which coupling the Fortran version HADVPPM, CUDA and HIP version of GPU-  
 297 HADVPPM. And then, the coupling computational performance of the Fortran version of  
 298 HADVPPM on the Intel Xeon E5-2682 v4 CPU and domestic CPU processor A, the CUDA version  
 299 of GPU-HADVPPM on the NVIDIA Tesla K40m and V100 GPU accelerators, and the HIP version  
 300 of GPU-HADVPPM on the domestic GPU-like accelerator A were compared under BJ, HN, and  
 301 ZY case. The simulation time in this section is 1 hour unless otherwise specified.

302 Table 5 listed the elapsed time and speedup of the different versions of HADVPPM on the CPU



303 processors and GPU accelerators for BJ, HN, and ZY cases. Using CUDA and HIP technology to  
 304 port HADVPPM from CPU to GPU can significantly improve its computational efficiency.  
 305 Moreover, the optimization of thread and block co-indexing is used to simultaneously compute the  
 306 grid point in the horizontal direction (Cao et al., 2023), the larger the computing scale, the more  
 307 obvious the acceleration. For example, for the BJ case, the elapsed time of HADVPPM on the  
 308 domestic CPU processor A and Intel Xeon E5-2682 v4 CPU was 57.8 and 37.7 seconds, and it takes  
 309 the only 29.6, 6.8, and 1.6 seconds when porting to the NVIDIA Tesla K40m GPU, the domestic  
 310 GPU-like accelerator A, and NVIDIA Tesla V100 GPU, with speedup of 2.0x, 8.5x, and 36.1x. The  
 311 HN case has a slightly larger grid number, the acceleration of GPU-HADVPPM on NVIDIA Tesla  
 312 K40m GPU, the domestic GPU-like accelerator A, and NVIDIA Tesla V100 GPU is obvious which  
 313 were 2.7x, 11.5x, and 41.8x, respectively. The ZY case had the largest number of grids in the three  
 314 cases and exceeded the memory of a single NVIDIA Tesla K40m GPU accelerator, so it was not  
 315 possible to test its elapsed time on it. But as far as the domestic GPU-like accelerator A and NVIDIA  
 316 Tesla V100 GPU are concerned, the ZY case gets 28.9x and 80.2x acceleration on it compared to  
 317 the domestic CPU processor A.

318 **Table 5.** The elapsed time and speedup of the Fortran version of HADVPPM on the Intel Xeon E5-2682 v4 CPU  
 319 and the domestic CPU processor A, the CUDA version of GPU-HADVPPM on the NVIDIA Tesla K40m GPU,  
 320 NVIDIA Tesla V100 GPU, and the HIP version of GPU-HADVPPM on the domestic GPU-like accelerator A for BJ,  
 321 HN, and ZY case. The unit of elapsed time is in seconds (s).

		BJ case		HN case		ZY case	
		Elapsed time (s)	Speedup	Elapsed time (s)	Speedup	Elapsed time (s)	Speedup
CPU processor	domestic CPU processor A	57.8	1.0x	71.1	1.0x	609.2	1.0x
	Intel Xeon E5-2682 v4 CPU	37.7	1.5x	48.1	1.5x	395.7	1.5x
GPU accelerator	NVIDIA Tesla K40m GPU	29.6	2.0x	26.3	2.7x	-	-
	domestic GPU-like	6.8	8.5x	6.2	11.5x	21.1	28.9x



accelerator							
A							
NVIDIA							
Tesla V100	1.6	36.1x	1.7	41.8x	7.6	80.2x	
GPU							

322 In the above experiments to test the coupling performance of GPU-HADVPPM on NVIDIA  
 323 GPU and domestic GPU-like accelerator, the data transfer time between CPU and GPU was not  
 324 considered. However, the communication bandwidth of data transfer between the CPU and GPU is  
 325 one of the most significant factors that restrict the performance of numerical model on the  
 326 heterogeneous cluster (Mielikainen et al., 2012; Mielikainen et al., 2013; Huang et al., 2013). To  
 327 exhibit the significant impact of CPU-GPU data transfer efficiency, the coupled computing  
 328 performance of GPU-HADVPPM with and without data transfer time for the BJ case is tested on  
 329 the domestic cluster A and B with the same DTK version 23.04 software environment. The elapsed  
 330 time of GPU-HADVPPM on domestic GPU-like accelerator A with and without taking into account  
 331 the data transfer time between CPU and GPU are 6.8 and 93.1 seconds, respectively, which means  
 332 that only 7.3% of the time is spent on GPU computing, and the rest of the time is spent on data  
 333 transfer. Although, the domestic cluster B upgrade the hardware component and network bandwidth,  
 334 and the elapsed time of GPU-HADVPPM on it with and without taking into account the data transfer  
 335 time are 5.7 and 23.9 seconds respectively, the GPU computing time is still only 23.8%. Optimizing  
 336 the data transfer efficiency between CPU and GPU is one of the most important directions for the  
 337 porting and adaptation of numerical models to heterogeneous clusters.

#### 338 4.3.2. CAMx-HIP model on the heterogeneous cluster

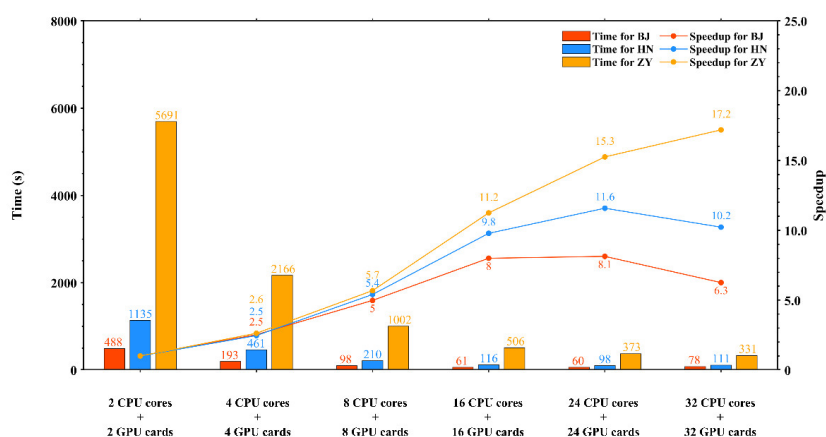
339 Generally, the super-large heterogeneous clusters have thousands of compute nodes which are  
 340 equipped with one or more GPUs on each node. To make full use of multiple GPUs, a parallel  
 341 architecture with an MPI and CUDA hybrid paradigm was implemented to improve the overall  
 342 computational performance of CAMx-CUDA model (Cao et al., 2023). In this studying, the hybrid  
 343 parallelism with an MPI and HIP paradigm was used to implement the HIP version of GPU-  
 344 HADVPPM run on multiple domestic GPU-like accelerators.

345 Fig.4 shows the total elapsed time and speedup of CAMx-HIP model which coupled with the  
 346 HIP version GPU-HADVPPM on the domestic cluster A under the BJ, HN, and ZY cases. The





347 simulation of above three cases for one hour took 488 seconds, 1135 seconds and 5691 seconds  
 348 respectively when launching two domestic CPU processors and two GPU-like accelerators. When  
 349 the number of CPUs and GPUs reaches 24, the speedup of BJ and HN cases reaches the maximum,  
 350 8.1x and 11.6x, respectively. In terms of the ZY case, it can achieve up to the 17.2 times speedup  
 351 when equipped with 32 domestic CPU processors and GPU-like accelerators.  
 352



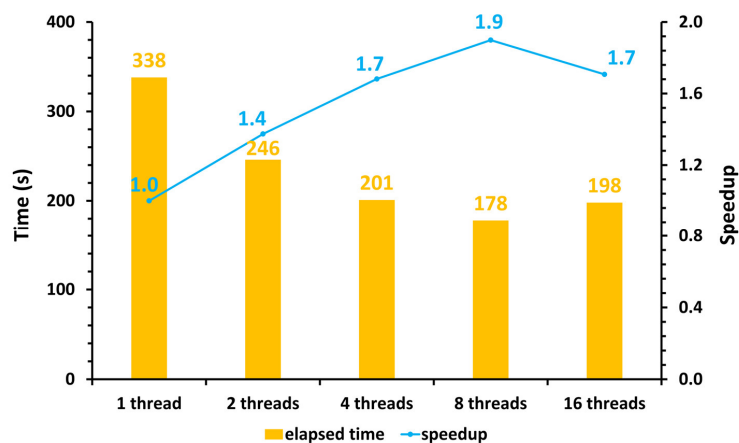
353  
 354 **Figure 4.** The total elapsed time and speedup of CAMx-HIP model on the domestic cluster A under the BJ, HN, and  
 355 ZY cases. The unit is in seconds (s).

356 The number of GPU accelerators in a single compute node is usually much smaller than the  
 357 number of CPU cores in the super-large heterogeneous cluster. Using the hybrid parallel paradigm  
 358 with MPI and HIP to configure one GPU accelerator for each CPU process results in idle computing  
 359 resources for the remaining CPU cores. Therefore, the multi-level hybrid parallelism scheme was  
 360 introduced to further improve the total computational performance of the CAMx-HIP model. As  
 361 described in the Sect. 3.2, the horizontal advection module is accelerated by MPI and HIP  
 362 technology and the other modules which runs on the CPU are accelerated by MPI and OMP under  
 363 the framework of the multi-level hybrid parallelism.

364 The ZY case achieved the maximum speed-up when launching the 32 domestic CPU  
 365 processors and GPU-like accelerators. In the same configuration, Fig. 5 shows the total elapsed time  
 366 and speedup of CAMx-HIP model when further implementing the multi-level hybrid parallelism on



367 the domestic cluster A. The AEs of the simulation results between the CAMx-HIP model and  
368 CAMx-HIP model with the OMP technology is within  $\pm 0.04$  ppbV, and the specified results are  
369 shown in Figure S1. As the number of threads increases, the elapsed time of CAMx-HIP model is  
370 further reduced. When a CPU core launching 8 threads, the one-hour integration time in CAMx-  
371 HIP model has been reduced from 338 seconds to 178 seconds, with a maximum acceleration of  
372 1.9x.



373  
374 **Figure 5.** The total elapsed time and speedup of CAMx-HIP model when implementing the multi-level hybrid  
375 parallelism in the ZY case. The unit is in seconds (s).

## 376 5. Conclusions and discussion

377 GPUs have become an essential part of providing processing power for high performance  
378 computing application, especially in the field of geoscience numerical models, implementing super-  
379 large scale parallel computing of numerical models on GPUs has become one of the significant  
380 directions of its future development. In this studying, the ROCm HIP technology was implemented  
381 to port the GPU-HADVPPM from the NVIDIA GPUs to China's domestically GPU-like  
382 accelerators, and further introduced the multi-level hybrid parallelism scheme to improve the total  
383 computational performance of the CAMx-HIP model on the China's domestically heterogeneous  
384 cluster.



385 The consistency of model simulation results is a significant prerequisite for heterogeneous  
386 porting, although the experimental results show that the simulation difference of CAMx-CUDA and  
387 CAMx-HIP models are within an acceptable range, the simulation difference of CAMx-HIP model  
388 is smaller, which indicates that the domestic GPU-like accelerator is more accuracy for scientific  
389 computing in the field of geoscience numerical models. Moreover, the BJ, HN, and ZY test cases  
390 can achieve 8.5x, 11.5x, and 28.9x speedup, respectively, when the GPU-HADVPPM program is  
391 ported to the domestic GPU-like accelerator A. And the larger the computing scale, the more obvious  
392 the acceleration effect of the GPU-HADVPPM program, which means that the GPU is more suitable  
393 for super-large scale parallel computing. The data transfer bandwidth between CPU and GPU is one  
394 of the most important factors affecting the computational efficiency of numerical model in  
395 heterogeneous clusters, the elapsed time of GPU-HADVPPM program on GPU only accounts for  
396 7.3% and 23.8% when considering the data transfer time between CPU and GPU on the domestic  
397 cluster A and B. Therefore, optimizing the data transfer efficiency between CPU and GPU is one of  
398 the important directions for the porting and adaptation of geoscience numerical models on  
399 heterogeneous clusters in the future.

400 There is still potential to further improve the computational efficiency of the CAMx-HIP model  
401 in the further. First, improve the data transfer efficiency of GPU-HADVPPM between the CPU and  
402 the GPU and reduce the data transfer time. Secondly, increase the proportion of HIP C code in  
403 CAMx-HIP model on the domestic GPU-like accelerator, and port other modules of CAMx-HIP  
404 model to the domestic GPU-like accelerator for computing. Finally, the data type of some variables  
405 can be changed from double precision to single precision, and the mixing-precision method is used  
406 to further improve the CAMx-HIP computing performance.

407

408

409 *Code and data availability.* The source codes of CAMx version 6.10 are available at <https://camx->  
410 [wp.azurewebsites.net/download/source/](https://camx-wp.azurewebsites.net/download/source/) (ENVIRON, 2023). The datasets related to this paper and  
411 the CAMx-HIP codes are available online via ZENODO  
412 (<https://doi.org/10.5281/zenodo.10158214>), and the CAMx-CUDA code is available online via  
413 ZENODO (<https://doi.org/10.5281/zenodo.7765218>, Cao et al., 2023).



414

415 *Author contributions.* KC and QW conducted the simulation and prepared the materials. QW, LiW  
416 and LaW planned and organized the project. KC, QW, HG, HW, XT and LL refactored and  
417 optimized the codes. LiW, NW, HC, and DL collected and prepared the data for the simulation. KC,  
418 HW, QW, and HG validated and discussed the model results. KC, QW, LiW, NW, XT, HG, and LaW  
419 took part in the discussion.

420

421 *Competing interests.* The authors declare that they have no conflict of interest.

422

423 *Acknowledgements.* The National Key R&D Program of China (grant no. 2020YFA0607804), the  
424 National Supercomputing Center in Zhengzhou Innovation Ecosystem Construction Technology  
425 Special Program (grant no. 201400210700), GHfund A (grant no. 202302017828), and the Beijing  
426 Advanced Innovation Program for Land Surface funded this work. The authors would like to thank  
427 the High Performance Scientific Computing Center (HSCC) of Beijing Normal University for  
428 providing some high-performance computing environment and technical support.

429

## 430 **Reference**

431 Alvanos, M. and Christoudias, T.: GPU-accelerated atmospheric chemical kinetics in the  
432 ECHAM/MESy (EMAC) Earth system model (version 2.52), Geoscientific Model  
433 Development, 10, 3679-3693, 10.5194/gmd-10-3679-2017, 2017.

434 AMD: ROCm Documentation Release 5.7.1,  
435 [https://rocm.docs.amd.com/\\_downloads/en/latest/pdf/](https://rocm.docs.amd.com/_downloads/en/latest/pdf/) (last access: 20 October 2023), 2023.

436 Bott, A.: A Positive Definite Advection Scheme Obtained by Nonlinear Renormalization of the  
437 Advective Fluxes, Monthly Weather Review - MON WEATHER REV, 117, 10.1175/1520-  
438 0493(1989)117<1006:APDASO>2.0.CO;2, 1989.

439 Cao, K., Wu, Q., Wang, L., Wang, N., Cheng, H., Tang, X., Li, D., and Wang, L.: GPU-HADVPPM  
440 V1.0: a high-efficiency parallel GPU design of the piecewise parabolic method (PPM) for  
441 horizontal advection in an air quality model (CAMx V6.10), Geosci. Model Dev., 16, 4367-



442 4383, 10.5194/gmd-16-4367-2023, 2023.

443 Cao, K., Wu, Q., Wang, L., Wang, N., Cheng, H., Tang, X., Li, D., and Wang, L.: The dataset of the  
444 manuscript “GPUHADVPPM V1.0: high-efficient parallel GPU design of the Piecewise  
445 Parabolic Method (PPM) for horizontal advection in air quality model (CAMx V6.10)”,  
446 Zenodo [data set], <https://doi.org/10.5281/zenodo.7765218>, 2023.

447 Colella, P. and Woodward, P. R.: The Piecewise Parabolic Method (PPM) for gas-dynamical  
448 simulations, *Journal of Computational Physics*, 54, 174-201, [https://doi.org/10.1016/0021-](https://doi.org/10.1016/0021-9991(84)90143-8)  
449 9991(84)90143-8, 1984.

450 ENVIRON: User Guide for Comprehensive Air Quality Model with Extensions Version 6.1,  
451 [https://camx-wp.azurewebsites.net/Files/CAMxUsersGuide\\_v6.10.pdf](https://camx-wp.azurewebsites.net/Files/CAMxUsersGuide_v6.10.pdf) (last access: 20  
452 October 2023), 2014.

453 ENVIRON: CAMx version 6.1, ENVIRON [code], available at: [https://camx-](https://camx-wp.azurewebsites.net/download/source/)  
454 wp.azurewebsites.net/download/source/, last access: 20 October 2023.

455 Huang, M., Huang, B., Mielikainen, J., Huang, H. L. A., Goldberg, M. D., and Mehta, A.: Further  
456 Improvement on GPU Based Parallel Implementation of WRF 5-Layer Thermal Diffusion  
457 Scheme, in: 2013 International Conference on Parallel and Distributed Systems, Seoul, South  
458 Korea, 15–18 December 013, <https://doi.org/10.1109/icpads.2013.126>, 2013.

459 Linford, J. C., Michalakes, J., Vachharajani, M., and Sandu, A.: Automatic Generation of Multicore  
460 Chemical Kernels, *IEEE Transactions on Parallel and Distributed Systems*, 22, 119-131,  
461 10.1109/tpds.2010.106, 2011.

462 Mielikainen, J., Huang, B., Huang, H.-L. A., and Goldberg, M. D.: GPU Implementation of Stony  
463 Brook University 5-Class Cloud Microphysics Scheme in the WRF, *IEEE Journal of Selected*  
464 *Topics in Applied Earth Observations and Remote Sensing*, 5, 625-633,  
465 10.1109/jstars.2011.2175707, 2012.

466 Mielikainen, J., Huang, B., Wang, J., Allen Huang, H. L., and Goldberg, M. D.: Compute unified  
467 device architecture (CUDA)-based parallelization of WRF Kessler cloud microphysics scheme,  
468 *Computers & Geosciences*, 52, 292-299, 10.1016/j.cageo.2012.10.006, 2013.

469 NVIDIA: CUDA C++ Programming Guide Version 10.2,  
470 [https://docs.nvidia.com/cuda/archive/10.2/pdf/CUDA\\_C\\_Programming\\_Guide.pdf](https://docs.nvidia.com/cuda/archive/10.2/pdf/CUDA_C_Programming_Guide.pdf) (last



471 access: 20 October 2023), 2020.

472 Odman, M. and Ingram, C.: Multiscale Air Quality Simulation Platform (MAQSIP): Source Code  
473 Documentation and Validation, 1996.

474 Sun, J., Fu, J. S., Drake, J. B., Zhu, Q., Haidar, A., Gates, M., Tomov, S., and Dongarra, J.:  
475 Computational Benefit of GPU Optimization for the Atmospheric Chemistry Modeling,  
476 Journal of Advances in Modeling Earth Systems, 10, 1952-1969,  
477 <https://doi.org/10.1029/2018MS001276>, 2018.

478 Wang, P., Jiang, J., Lin, P., Ding, M., Wei, J., Zhang, F., Zhao, L., Li, Y., Yu, Z., Zheng, W., Yu, Y.,  
479 Chi, X., and Liu, H.: The GPU version of LASG/IAP Climate System Ocean Model version 3  
480 (LICOM3) under the heterogeneous-compute interface for portability (HIP) framework and its  
481 large-scale application, GEOSCIENTIFIC MODEL DEVELOPMENT, 14, 2781-2799,  
482 [10.5194/gmd-14-2781-2021](https://doi.org/10.5194/gmd-14-2781-2021), 2021.